



Visible light responsive S-Doped TiO₂ nanoparticles: synthesis, characterization and photocatalytic degradation of pollutants

Nidhi Sharotri¹ · Shivali Gupta² · Dhiraj Sud²

Received: 20 July 2021 / Accepted: 27 January 2022 / Published online: 18 February 2022
© The Author(s), under exclusive licence to Springer Nature Switzerland AG 2022

Abstract

Heterogeneous catalyst (TiO₂) based reactions have appeared as an important destructive methodology for the removal of various organic and inorganic contaminants. The unique properties of TiO₂ such as stability against photo corrosion, sufficient bandgap, easy accessibility, and self-surface cleaning make it more promising photocatalyst. However, one of the major limitations of TiO₂ is broader bandgap that makes it active only in the UV region. Thus the current emphasis of research in photocatalysis field is to make titanium dioxide, a solar light receptive photocatalyst. The present study reports a greener synthetic approach for the synthesis of sulphur doped TiO₂ using titanium isopropoxide and thiophenol as an initial precursors. The synthesized photocatalysts were calcinated at different temperatures and depicted by using SEM–EDS, HR-TEM, PL, UV–Vis, FT-IR, XPS and XRD. The photocatalytic response was examined for various model compounds such as Rhodamine 6G (synthetic dye), Quinalphos (an organophosphate pesticide), and Diclofenac (a pharmaceutical waste).

Keywords TiO₂ · Photocatalysis · Rhodamine 6 G · Quinalphos · Diclofenac

Introduction

The last century witnessed the dilemma faced by mankind to choose between the twin intricate issues of economic development and environmental protection. However, the balance was shifted toward economic development, which led to rapid industrialization, mining and metallurgical operations, and advancement in agricultural practices. However, from the mid of twentieth century, scientists and economists have realized the pitfalls of the narrow approach followed by the visible impacts on the fast degradation of every segment of the environment. From the 1970s onwards the research focus was diverted toward the development of environment-friendly technologies particularly in the areas of sustainable energy formation and environmental issues. One such technology is the advanced oxidation process (AOPs), which provides solutions for the treatment of surface wastewater

containing hardly recyclable anthropogenic substances, disinfection of drinking water, and air purification [1].

U.S. EPA has certified that AOPs are the best available technology that meets the standards that are required for harmless and contaminant-free discharge process [2]. Hence, following the above-mentioned technology, heterogeneous photocatalysis has come across as a promising technique for the elimination of hazardous contaminants from the environment using semiconductors as a photocatalyst in solar light or UV light. Out of several semiconductor materials, titanium dioxide (TiO₂) has emerged as the utmost effective photocatalyst because of its biological and chemical inertness, non-toxicity, hydrophilicity, resistance to chemical, and photo-corrosion, and low cost. In ambient conditions, TiO₂ is more stable than other photocatalysts and can be recycled [3–5]. TiO₂ has a normal bandgap for the rutile phase (3.0 eV) and anatase phase (3.2 eV), therefore, a vast energy difference between the valance and conduction level is responsible for its use in the UV light. The anatase phase is thermally less stable due to its zig-zag motion than rutile phase which is more stable at various temperature and pressure conditions due to its linear chain. The phase transformation from anatase to rutile form takes place at 700–1000 °C. Rutile has a small bandgap, which indicates that a bigger portion of solar radiation can stimulate bandgap excitation.

✉ Nidhi Sharotri
nidhisliet11@gmail.com

¹ Department of Chemistry, Sri Sai University, Palampur, Himachal Pradesh 176061, India

² Department of Chemistry, Sant Longowal Institute of Engineering and Technology, Longowal (Deemed University), Sangrur, Punjab 148106, India

Thus to adjust the bandgap, several methods are available but doping is one of the most widely used techniques. This is because doping may enhance the surface area and crystallinity of the synthesized nanoparticle by decreasing the size of crystal. Doping leads to bathochromic shift due to which optical response changes that are decrease in band gap results in the absorption shift toward the visible region. Anionic doping is considered the most successful method to synthesize TiO_2 with higher photocatalytic efficiency under visible light. In an anion doping, the p-state of an anion (N, S, or C) mix with O_{2p_z} that helps in shifting the valence level edge upwards, thus helping in narrowing the gap of TiO_2 [6, 7]. Various cationic dopants (Mn, Co, Ni, Cu, Fe, and Zn) turned out to be a worthy approach to improve the photocatalytic efficiency of the photocatalyst by transferring the absorption edge toward the higher wavelength region [8–10].

The three fundamental approaches, which enhance the photocatalytic activity, are bandgap alteration, elongation of excitation wavelength, and extension in recombination time of charge-carrier. There are several modes to achieve the above parameters include chemical modification on surface, metal, or non-metal doping of photocatalyst, and coupled systems [11–16].

Synthetic compounds such as phenols, herbicides, dyes, pesticides, fertilizers, and surfactants find their way into the environment. These compounds are very toxic to human health. Their elimination from the environment has become a primary concern for researchers.

The synthesized nanoparticles have various properties like a high content of anatase phase, greater surface area, and lesser crystalline size, which increase the rate of photocatalytic reaction. Tongpool et al. [17] synthesized S-doped TiO_2 catalyst and their study showed that the hydrophilicity of photocatalyst and thiourea solvents played a very important role in the incorporation of sulphur into TiO_2 structure and photocatalytic activity. Doping also enhanced the absorption edge toward visible light by hindering the grain growth and resulted in increased surface area. Zhou et al. [18] have used a simple method for the preparation of photoactive N, C, S-tridoped TiO_2 with improved photocatalytic efficiency as compared to bare TiO_2 . Sulphur doped TiO_2 catalysts having crystal size of 8–10 nm were synthesized by using the sol–gel method. XRD results showed that anatase phase exists for undoped and doped photocatalysts at 500 °C. When calcination temperature was varied, rutile phase was observed for undoped photocatalysts at 650–700 °C and for doped photocatalyst at 750 °C [19]. Ivanov et al. synthesized sulfur and carbon co-doped TiO_2 nanoparticles via one-step synthetic route with particle sizes between 15 and 40 nm. The synthesized nanoparticles showed an effective photocatalytic response for the degradation of rhodamine B, methylene blue, etc. [20]. Ramacharyulu et al. synthesized

N and S-doped TiO_2 nanocatalysts using a sol–gel method further accompanied by hydrothermal method [21].

Sulphur-modified TiO_2 nanoparticles have been generated in a vast number of studies, as evidenced by the literature. The produced nanoparticles have demonstrated independent degrading efficiency against pesticides, dyes, toxins, and other pollutants. To our knowledge, no publications exist where S-doped TiO_2 has demonstrated efficient degradation against dye, pesticides, and drugs simultaneously.

Herein, sulphur doped TiO_2 nanoparticles are synthesized using a greener approach. Ultrasonic assisted S- TiO_2 lies in the particle size range of 55–19 nm. Various characterization techniques such as SEM, EDS, FTIR, HR-TEM, and XRD have provided insight knowledge of structure, morphology, particle size, and shape of the nanoparticles. The effect of calcination temperature on the above-mentioned parameters has been discussed in detail. Compared to bare TiO_2 , S-doped TiO_2 has proved to be more efficient in photocatalytic activity as the presence of sulphur leads to a decrease in the bandgap energy and hence made it more efficient in visible light. In terms of its application part, the as-synthesized nanoparticles have shown great efficiency in the degradation of a pharmaceutical drug (Diclofenac), synthetic dye (Rhodamine 6G), and pesticide (Quinalphos).

Materials and methods

Chemicals

The chemicals used for synthesis purposes are titanium isopropoxide, ethanol, ammonium hydroxide, and thiophenol. As model compounds for photocatalytic degradation experiment Rhodamine 6G, Quinalphos, and Diclofenac are used. All the chemicals were of analytical grade. Millipore water was used for solution preparation. Degussa P25 TiO_2 used for comparative conclusions was procured from Degussa Company, Germany; having 30% rutile and 70% anatase crystals with an average particle size of 30 nm. The BET surface area of TiO_2 was $50 \pm 15 \text{ m}^2/\text{g}$.

Equipment and Instruments

The crystallite size, phase, and crystal structure of the synthesized photocatalyst were investigated by using x-ray diffraction (XRD) technique. The XRD results were obtained by using Rigaku 2000® using a $\text{CuK}\alpha$ ($\lambda = 1.5418$ angstroms) emission source ranging from 5 to 90 degrees having a step size of 0.1 with 4 s of collection time. JSM-6610/EO named energy-dispersive x-ray microanalysis (EDXMA) instrument was used to determine the elemental composition of synthesized catalyst. High Resolution-TEM (MOR-GAGNI-268 E) was used to study the inner structure using

a fine powder-coated copper grid glazed with carbon. An FT-IR spectrum was analyzed by Model- RZX, Perkin Elmer. Sampling was done by using KBr disc (1:100, sample/KBr) with a total of 16 scans per sample at a resolution of 4 cm^{-1} within $4000\text{--}400\text{ cm}^{-1}$ range. UV–VIS absorption spectra were recorded on Shimadzu UV 1800. Photoluminescence (PL) spectroscopy helped record photoemission spectra of samples with spectrometer RF-5301 (Shimadzu). An ultrasonication bath of brand named Microfil from LINCO having model number GB/2500B of 40 kHz frequency range was used for the preparation of evenly distributed metal oxide photocatalyst.

Synthesis of photocatalyst

Pure TiO_2

Titanium isopropoxide (2.84 gm) was dissolved in 20 ml of ethanol. NH_4OH (10%) solution was further added dropwise to the solution with continuous stirring, which results in precipitation. The above-formed resultant mixture was magnetically stirred for about half an hour. After that, the resultant mixture was sonicated for 40 min in an ultrasonic bath, and later the mixture was again stirred for an hour and thereafter kept overnight. The prepared particles were first filtered and then dehydrated in a hot air oven for 2 h at $100\text{ }^\circ\text{C}$.

Synthetic route of sulphur doped nano photocatalysts

S-doped TiO_2 was synthesized by mixing 1 M titanium isopropoxide (2.84 g) and 0.1 M thiophenol (as a sulphur precursor) in ethanol (20 ml). The mixture solution was magnetically stirred for half an hour and this further lead to the addition of 10% NH_4OH till precipitation occurs with continuous stirring. After that, the precipitates were again stirred for an hour. Now, the precipitates were ultrasonicated for 40 min in an ultrasonic bath and afterward were stirred again for an hour. Resultant precipitates were kept overnight and thereafter were filtered and washed with ethanol. The synthesized precipitates were firstly dried in an oven at $100\text{ }^\circ\text{C}$ for 2 h and thereafter calcinated at different temperatures i.e., 350, 550, 750, and $1050\text{ }^\circ\text{C}$.

Photocatalytic degradation experiment

A photocatalytic reactor was devised for the execution of degradation experiments having LED bulbs (Phillips) each of 12 W. The photocatalysis reaction was studied by using specially designed reaction vessels of 500 ml capacity. Aerators were used for aeration and magnetic stirrers did constant stirring of solution. The temperature of the reactor was kept constant by flowing water in a jacketed wall of the

reactor. The millipore syringe filters ($0.22\text{ }\mu\text{m}$) were used for filtration of the samples. A pH meter (Thermo Orion 920A) was used to analyze the acidity/basicity of the solution and the pH was adjusted by adding NaOH or HCl. The photocatalytic degradation of pollutants (R6G, Quinalphos, and Diclofenac) was performed by taking 50 ml of pollutant and 50 mg of as-synthesized nano photocatalyst. The resulting mixture was irradiated using LED bulb of an appropriate wavelength and the solution was stirred magnetically and aerated constantly. The degradation was determined by measuring the UV–VIS absorption spectrum [21]. The percentage degradation was estimated by using formula as follows:

$$\text{Efficiency (\%)} = (A_0 - A) / A_0 \times 100 \quad (1)$$

Results and discussion

This section covers the synthesis, characterization, and photocatalytic response of the synthesized particles. S- TiO_2 was synthesized by an eco-friendlier approach using ultrasonic irradiations. Various physicochemical methods such as XRD, EDX, TEM, UV–VIS, FTIR, band gap, and PL were engrossed for characterizing synthesized catalysts. Rhodamine 6G (synthetic dye), Quinalphos (an organophosphate pesticide), and Diclofenac (pharmaceutical waste) were used as model compounds for analyzing the photocatalytic efficiency of various synthesized catalysts.

Synthesis of S-doped TiO_2

S-doped TiO_2 nano photocatalyst was prepared by reacting titanium isopropoxide with thiophenol under ultrasonic irradiation. The catalysts synthesized at 350, 550 750, and $1050\text{ }^\circ\text{C}$ were labelled as ST-350, ST-550, ST-750, and ST-1050, respectively. To optimize various reaction conditions the catalyst was manufactured by varying the reaction time for ultrasonication and by employing different solvents. The optimized ultrasonication time obtained was 40 min based on the surface morphology and product yield.

X-ray diffraction (XRD) pattern of S-doped TiO_2

The XRD data was used to determine the crystal structure and phase of the prepared photocatalyst. The x-ray diffraction results of prepared catalyst labelled Undoped- TiO_2 , ST-550, ST-750, and ST-1050 are shown in Fig. 1. In the case of undoped- TiO_2 main peak was seen at 25.25° and matched with JCPDS card number 01–073–1764. The XRD pattern of synthesized ST-350 showed that there was no peak, which confirmed the amorphous nature of the catalyst.

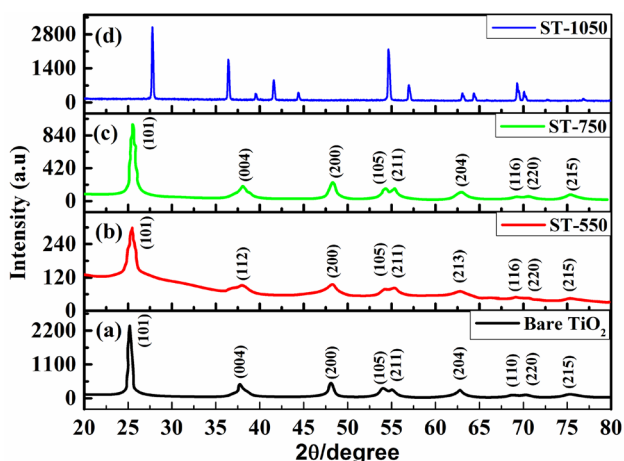


Fig. 1 a XRD patterns of bare TiO_2 and XRD pattern of S-doped TiO_2 nanoparticles, b ST-550, c ST-750 and d ST-1050

Whereas, in the case of ST-550 strong diffraction peaks at 10.2° , 25.5° , 36.1° , 37.9° , 48.1° , 55.2° , 62.7° were observed and matched with JCPDS card number 01–073-1764.

The XRD spectra of ST-750 showed peaks at 15.1° , 25.5° , 37.1° , 37.02° , 38.1° , 55.2° , 62.8° , confirming the appearance of anatase phase, which indicates that at 750°C delay in the phase transformation was observed [22]. The obtained pattern confirmed that anatase phase is the main phase as matched with ICDD card number 01–073-1764. However, at 1050°C the observed peaks at 27.7 , 36.4 , 39.5 , 41.5 , 44.3 , 54.6 , 56.9 , 64.3 , 69.3 , 70.0 ,

72.7 and 76.8 confirmed complete anatase to rutile phase transformation. This observed data was matched with ICDD card 01–070-7347, hence confirming the appearance of the rutile phase as the main phase at 1050°C .

The crystallite size (average) and the lattice strain have been analyzed by employing Scherer's Eq. (2) [23] and lattice strain equation [6] for S-doped TiO_2 nanoparticles calcinated at different temperatures.

$$D = k\lambda/\beta\cos\theta \quad (2)$$

where D is the crystal size of the catalyst, $K=0.89$, λ is the x-ray wavelength, β the full width at half the maximum of the catalyst, and θ is the diffraction angle.

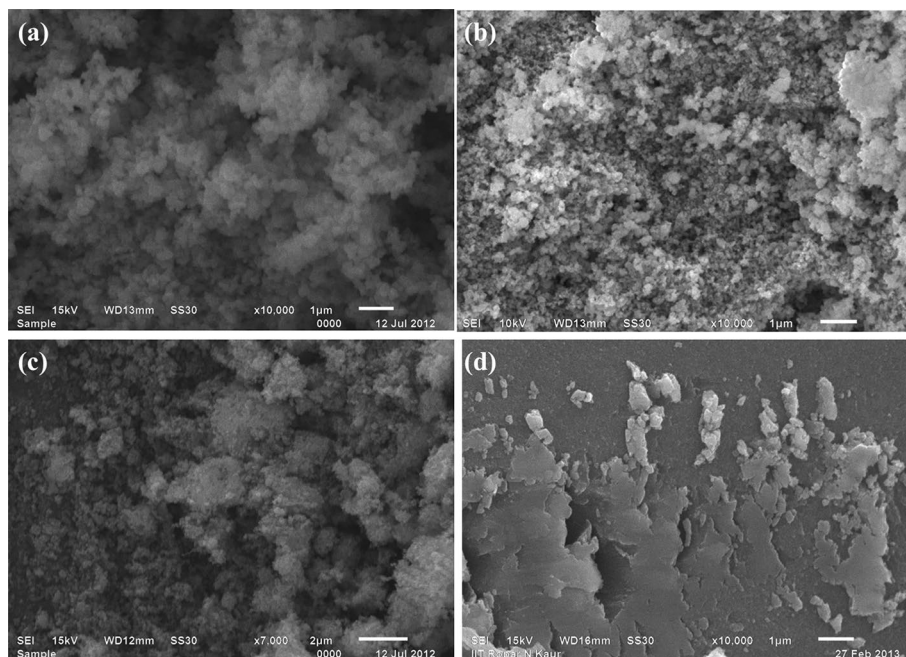
The results confirmed that the average crystallite size (23.1 nm , 42.4 nm , 36.5 nm) and lattice strain (0.0017 , 0.0023 , 0.002) were found to be for ST-550, ST-750, and ST-1050, respectively.

Elemental composition and Morphological studies of the synthesized photocatalyst

SEM

The surface structure and composition of the S-doped TiO_2 nanoparticles calcinated at 550°C (ST-550) have been studied by using the SEM technique as shown in Fig. 2b. The results confirm the formation of uniformly agglomerated nanoparticles with $0.33\text{ weight}\%$ of sulfur onto the lattice of TiO_2 .

Fig. 2 SEM images of a ST-350, b ST-550, c ST-750 and d ST-1050



Solvent effect on surface morphology

The solvents used during ultrasonication-induced synthesis had a great impact on the crystallite size and surface morphology. The variation in surface morphology was studied by synthesizing catalysts with different solvents such as butanol, isopropyl alcohol, ethanol, and methanol as shown in Fig. 2. The result confirmed that as the molecular weight of the solvent increases, the particle size of the synthesized catalyst also increases, having trend methanol < ethanol < isopropyl alcohol < n-butanol [24]. This sequence may result due to higher surface tension and greater solvent viscosity, which constrained the cavitations. The rock-like structures were obtained with higher molecular weight solvents such as isopropyl alcohol and butanol.

HR-TEM

The observed HR-TEM pattern depicted the distribution of uniformly arranged nanoporous particles having a particle size between 55 and 19 nm. In the case of ST-750 and ST-1050, the average particle size was nearer to 19 nm. The TEM image study demonstrates the successful synthesis of nano-sized photocatalyst by ultrasonic radiation, in the presence of thiophenol as a precursor of sulphur. The calcination temperatures affect the elemental composition and morphology of obtained catalyst as reflected from the TEM image shown in Fig. 3. TEM images showed that particle size decreases as the temperature increases. It was confirmed

from the images that particle size decreases from 53.90 to 19.59 nm, which was in the nano range.

Fourier transform infrared spectroscopy (FTIR) study of S-doped photocatalysts

The FTIR spectrum of prepared S-doped TiO₂ catalysts (ST-550) is shown in Fig. 4. The spectrum resulted in hydroxyl group stretching and bending vibration at 3304.96 cm⁻¹ and 1634.31 cm⁻¹ respectively, which may be because of a decrease in hydroxyl groups and water molecule concentration on the lattice of TiO₂.

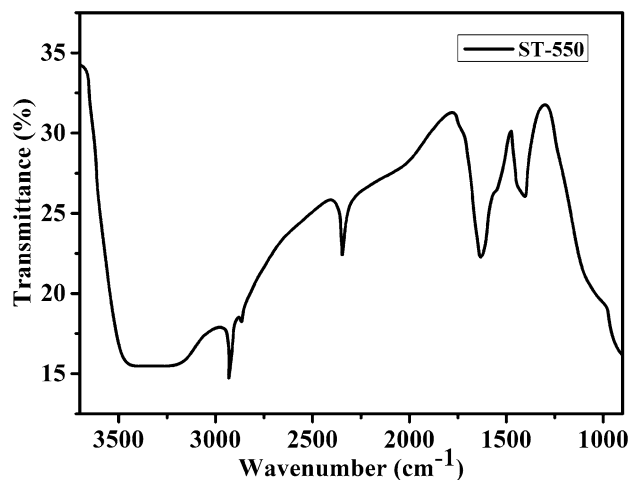
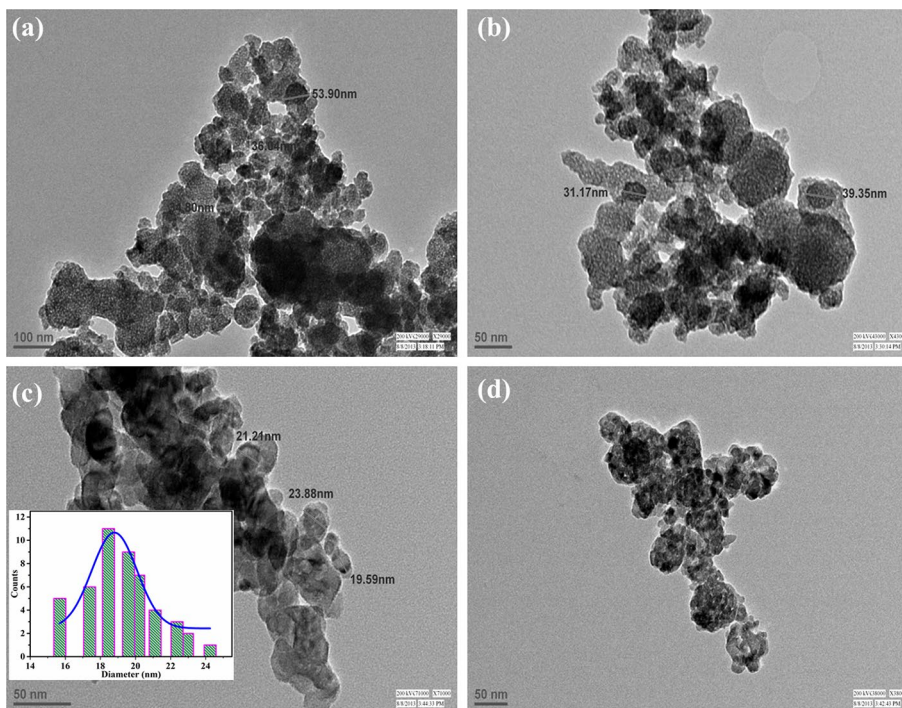


Fig. 4 FTIR spectra of ST-550

Fig. 3 HR-TEM images of S-doped TiO₂ nanoparticles **a** ST-350, **b** ST-550, **c** ST-750 and **d** ST-1050 (inset: particle size distribution image)



S = O stretching mode was observed at 1050.11 cm^{-1} . An intense peak at 789.54 cm^{-1} was observed, which occurs due to the vibration stretching mode of Ti–O [25, 26].

Ultraviolet–visible spectroscopy and bandgap study

UV–VIS spectra of S-doped TiO_2 , calcinated at different temperatures is shown in Fig. 5. The bandgap investigation was obtained by plotting graph between $E\text{ (h}\nu\text{)}$ vs $(\alpha\text{h}\nu)^{1/2}$ for synthesized S-doped TiO_2 as shown in Fig. 6. Hence,

Fig. 5 UV–Vis spectra of **a** ST-350, **b** ST-550, **c** ST-750 and **d** ST-1050

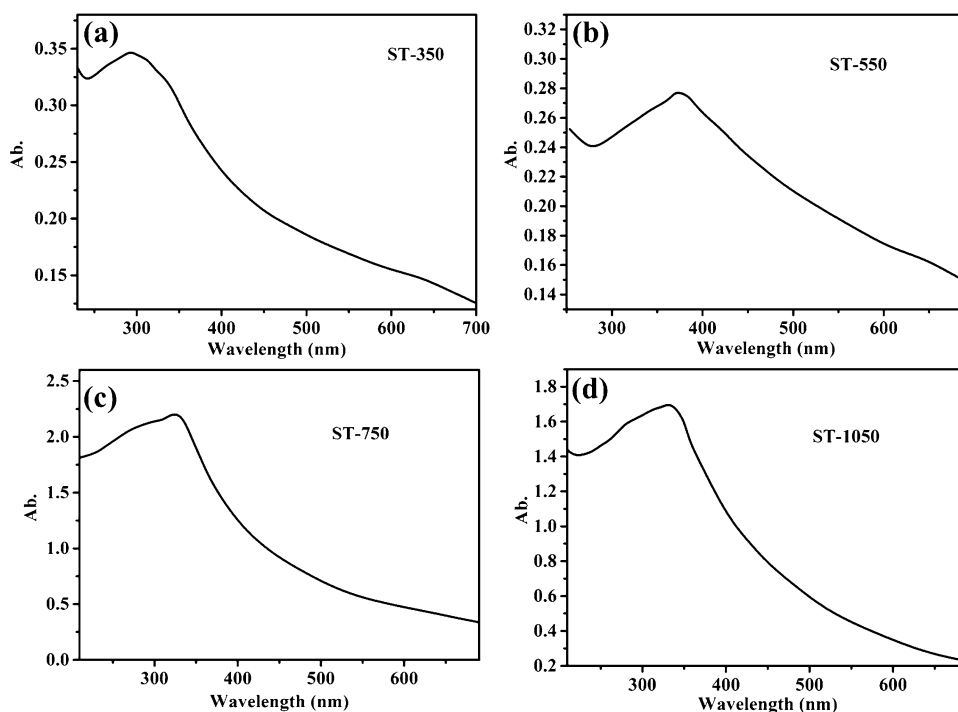
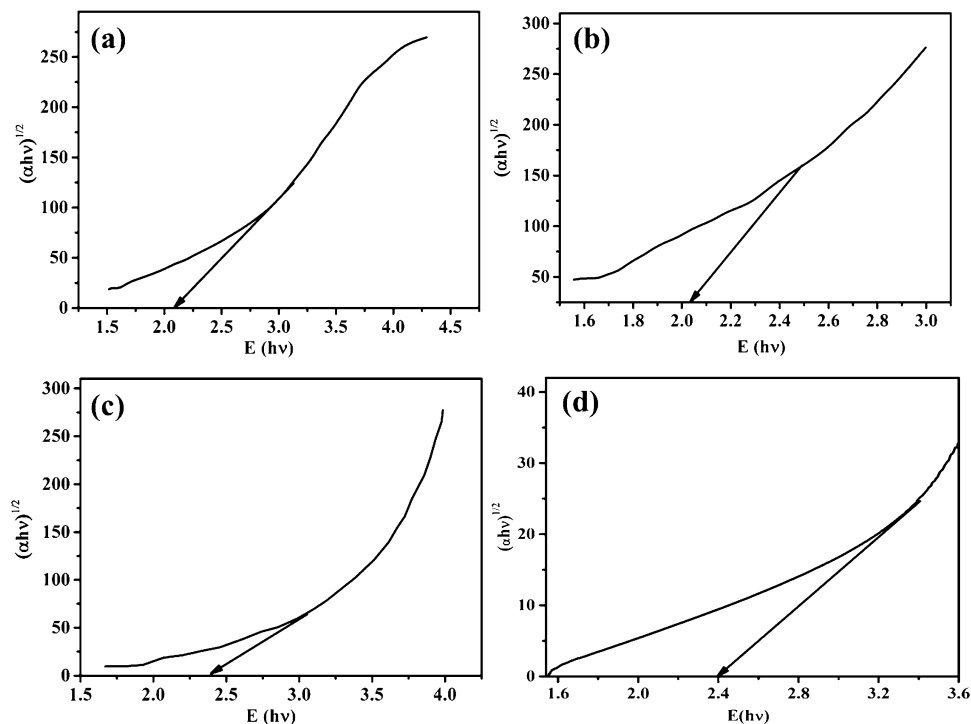


Fig. 6 Band gap studies of **a** ST-350, **b** ST-550, **c** ST-750 and **d** ST-1050

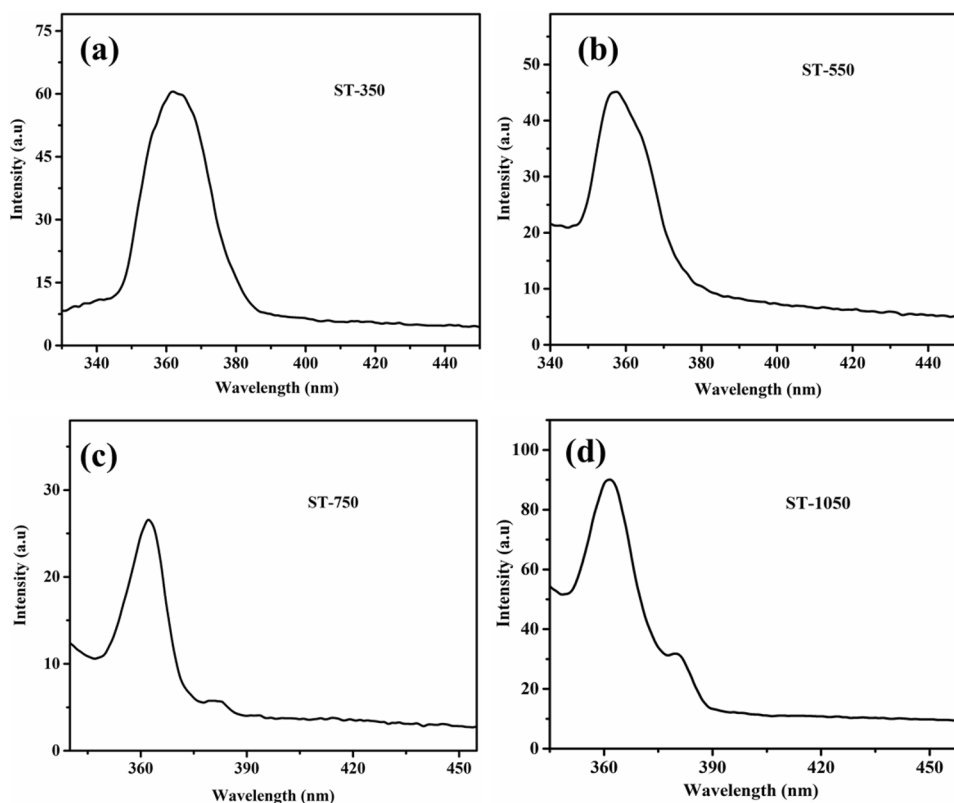


the calculated bandgap energy value was 2.21 eV, 2.03 eV, 2.02 eV and 2.3 eV for synthesized ST-350, ST-550, ST-750, and ST-1050, respectively. The results confirmed that the energy gap between valance level and conduction level decreases in comparison with the bandgap of pure TiO₂. So this study showed that sulphur doped photocatalyst has a narrow bandgap and the absorption edge has been shifted toward a higher wavelength, which may lead to the solar light-induced photocatalytic activity.

Photoluminescence spectra (PL) of synthesized S-doped TiO₂

Photoluminescence emission spectrum is extensively used to examine the efficacy of charge carrier trapping, transfer, migration, and also appropriate to understand the chance of electron–hole pairs recombination in semiconductors. The photoluminescence spectrum of ST-350 depicted the appearance of a weak emission peak at 310 nm and an intense peak at 360 nm. For ST-550, a single intense peak was observed at 370 nm. In the case of ST-750 and ST-1050, two peaks ranging between 360 nm–380 nm and 370–400 nm were observed, respectively (Fig. 7). The peak intensity initially decreases with an increase in calcination temperature from 350, 550, and 750 °C which was due to enhanced non-radiative recombination, and thereafter, the peak intensity increases again as temperature increases to 1050 °C.

Fig. 7 Fluorescence spectra of **a** ST-350, **b** ST-550, **c** ST-750 and **d** ST-1050



XPS study

XPS was known as a convenient characterization technique, which determined the chemical state of as-synthesized S-doped-TiO₂ nanoparticles. Figure 8a recorded the full-scale XPS spectrum of synthesized S-doped-TiO₂. The obtained results constitute Ti 2p, O 1s, S 2p, and C 1s spectra. Figure 8b represented the Ti 2p XPS spectrum in which the Ti 2p_{3/2} peak appeared at 458.7 eV and for Ti 2p_{1/2} peak centered at 465 eV, confirmed the existence of Ti⁴⁺ state. The O 1s spectra are shown in Fig. 8c in which band at 530.5 eV. Figure 8d represented the appearance of C 1s spectra with a band at 285.2 eV. Moreover, Fig. 8e showed S 2p spectra, which finally determined the successful doping of S into the TiO₂ lattice. A peak at 169.5 eV confirmed the substitution of S⁴⁺ ions in TiO₂ lattice. The total content of sulfur (atomic %) was found to be 2.21% [20, 27, 28].

Photocatalytic activity of S-doped TiO₂

For the optimal photocatalytic activity, nanoparticles must have a mixture of anatase phase and a small amount of rutile phase. With the increase in temperature, the rutile phase becomes the major phase of TiO₂ (For undoped = 650° and sulphur doped = 700–750°).

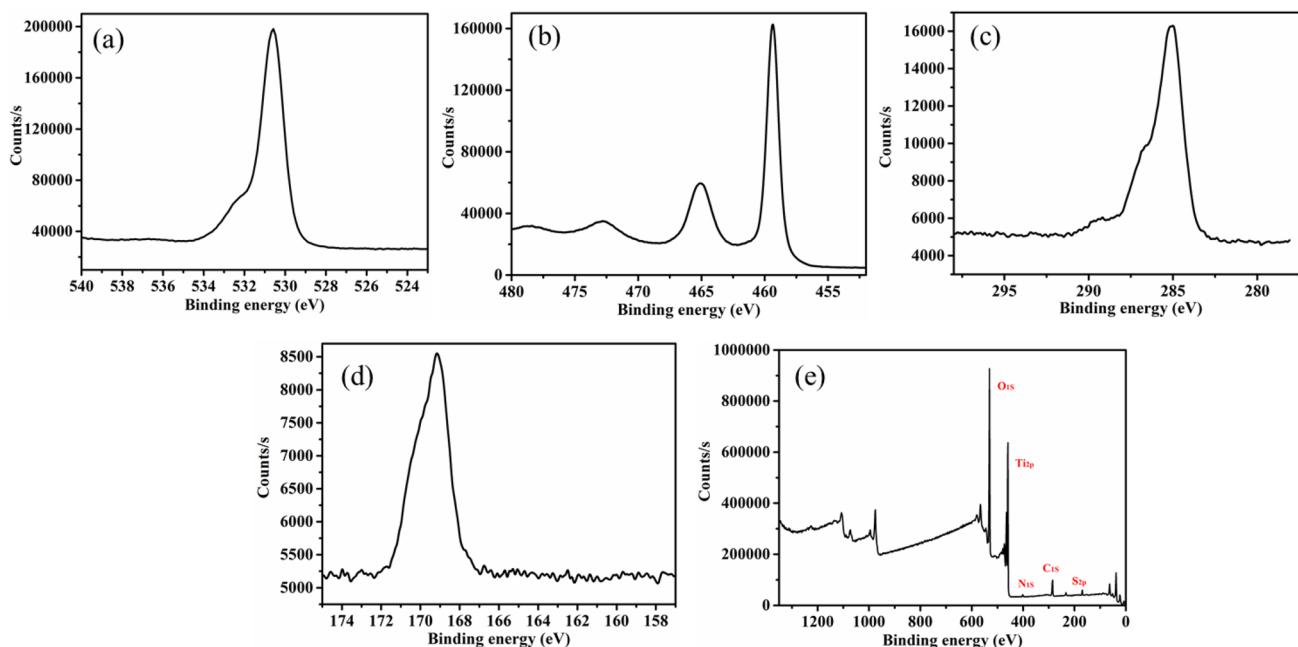


Fig. 8 XPS spectra of O1s (a), Ti2p (b), C1s (c), S2p (d), XPS survey (e) for the S-TiO₂ calcinated at 550 °C

Therefore, ST-550 was chosen for the photocatalytic activity over ST-750 in which the rutile phase dominates [23].

The photocatalytic response of prepared sulphur doped photocatalysts was assessed by degrading Rhodamine 6G, diclofenac, and quinalphos under visible light irradiation. These organic contaminants were released to the environment from sources such as paint stripping operations, by-products of agricultural chemicals, dyestuffs, and fireboard.

Photocatalytic degradation of R6G

Figure 9a showed the typical UV–VIS spectra (time-dependent) of R6G photo irradiation. R6G exhibited four bands at wavelength 347 nm, 275 nm, and 246 nm in the UV region and 526 nm in the visible region. But in the presence of S-TiO₂, absorption peaks corresponding to R6G started diminishing with increasing time, which indicates that the compound is degrading. Degradation efficiency was calculated to be 91.7% within four hours at wavelength 526 nm.

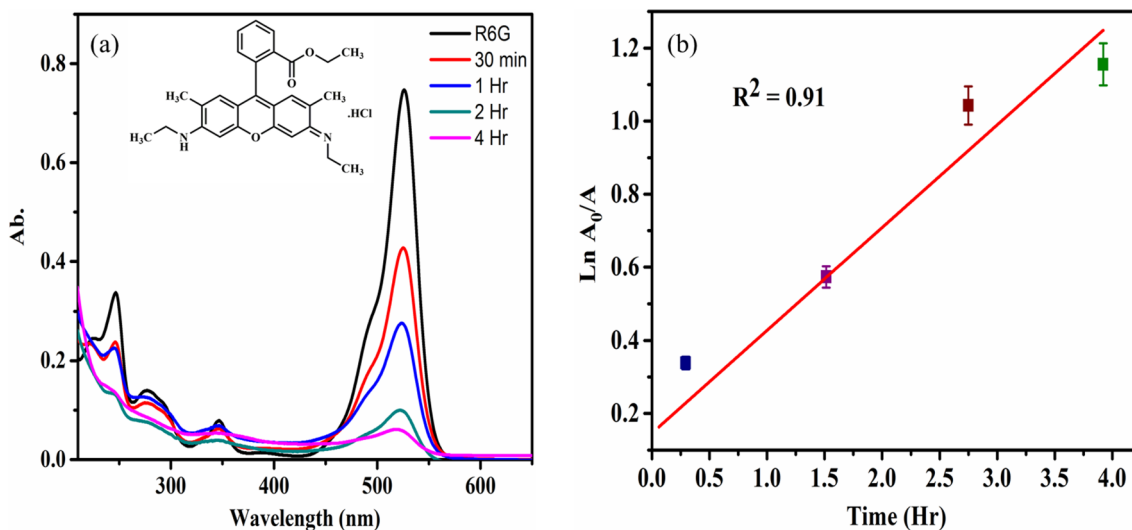


Fig. 9 UV–Vis time-dependent spectra (a) and Kinetic study plot (b) of photocatalytic degradation of R6G

Figure 9b shows the rate of disappearance of R6G under optimal conditions of pH and catalyst dose. The photocatalytic oxidation of organic compounds has been successfully obtained by using Langmuir–Hinshelwood kinetics. According to L–H model $-Dc/dt = Kk/(1 + KC)$, (where k is the reaction rate constant, C is the bulk solute concentration, K is the equilibrium adsorption constant and t represents time) for a low concentration of solute the value of KC is smaller than one that results in the pseudo-first-order equation. In $(A_0/A) = kt$, (where initial absorption is A_0 and absorption at any time is A , t is time), the photocatalytic degradation of R6G with TiO_2 confirmed a pseudo-first-order kinetic model [29]. Hence a straight line is obtained from semi-logarithmic plots of the concentration data. The value of R^2 comes out to be 0.952 and the rate constant was found to be 0.0587 min^{-1} for R6G.

The photocatalysis reaction of R6G has been observed under various experimental conditions as shown in Fig. 10a. For this, a blank experiment was executed under UV light (365 nm) in absence of catalyst, which confirmed that only 15% of R6G was degraded. About 20% of the R6G was degraded with TiO_2 in dark and 35% of the R6G is degraded with TiO_2 under white light (450 nm). While 40% degradation of R6G was observed in dark containing sulphur doped TiO_2 . Whereas 91.7% degradation was observed in white light containing S- TiO_2 . Turn over frequency was calculated to be $2 \times 10^7 \text{ mol}/(\text{mol} \cdot \text{min})$.

The pH effect on the % degradation of R6G under white light was studied over the range of 2–12 pH (Fig. 10b). Here, high degradation efficiency was observed at pH 9.

Photocatalytic Degradation of Quinalphos

The effect of calcination temperature on photocatalytic efficiency of S-doped TiO_2 was also investigated. The

photocatalytic activity of synthesized S-doped TiO_2 nano photocatalyst calcinated at different temperatures viz. 350, 550, 750, and 1050 °C were studied for the degradation of Quinalphos. The results showed 40.5, 85.7, 55.3, and 45.7% of quinalphos get degraded by using ST-350, ST-550, ST-750, and ST-1050, respectively. The maximum photocatalytic activity was shown by ST-550, thus selected for further studies.

Photocatalytic activity of the S-doped TiO_2 calcinated at 550 °C was assessed for degrading Quinalphos by varying reaction conditions (wavelength, pH, and photolysis reaction). The change in intensity of absorption maxima was used to identify the rate of % degradation.

The pesticide (Quinalphos) exhibited absorption maxima peaks at 320 nm and in the presence of S- TiO_2 , UV–Vis spectrum (time-dependent) of Quinalphos under visible light revealed a gradual decrease in absorption peak with 85.7% degradation of Quinalphos within 240 min as shown in Fig. 11a. The kinetics experiments proved that the apparent first-order kinetic model was used to evaluate the degradation of the pesticide (Fig. 11b). The value of the rate constant and correlation constant for the fitted line was 0.9636 min^{-1} and 0.0081, respectively.

Figure 12a represented the data of % degradation under four different experimental conditions that is red light (660 nm), undoped- TiO_2 / dark, ST-550/ dark, and ST-550/ red light. The blank experiment was accomplished under red light in the absence of catalyst showed 3.8% degradation only. When pesticide was degraded under dark conditions with undoped- TiO_2 only 23.5% degradation occurs. About 37.5% of the Quinalphos was degraded with ST-550 in dark conditions and 85.7% of Quinalphos degraded by using ST-550 under red light.

The pH effect on the % degradation was inspected in the range 2–10 as shown in Fig. 12b and the results confirmed

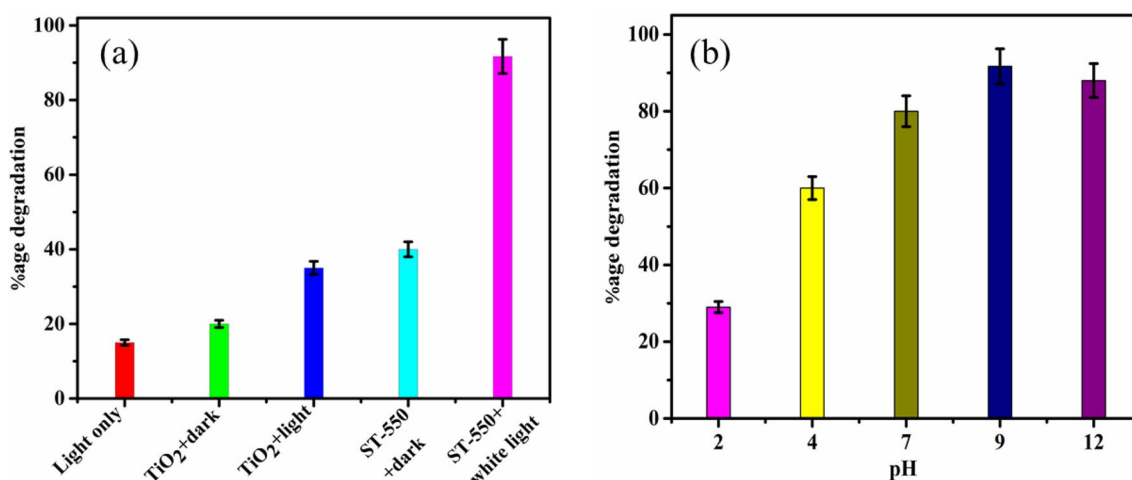


Fig. 10 Degradation efficiency of R6G **a** under different conditions and **b** pH effect under white light (450 nm)

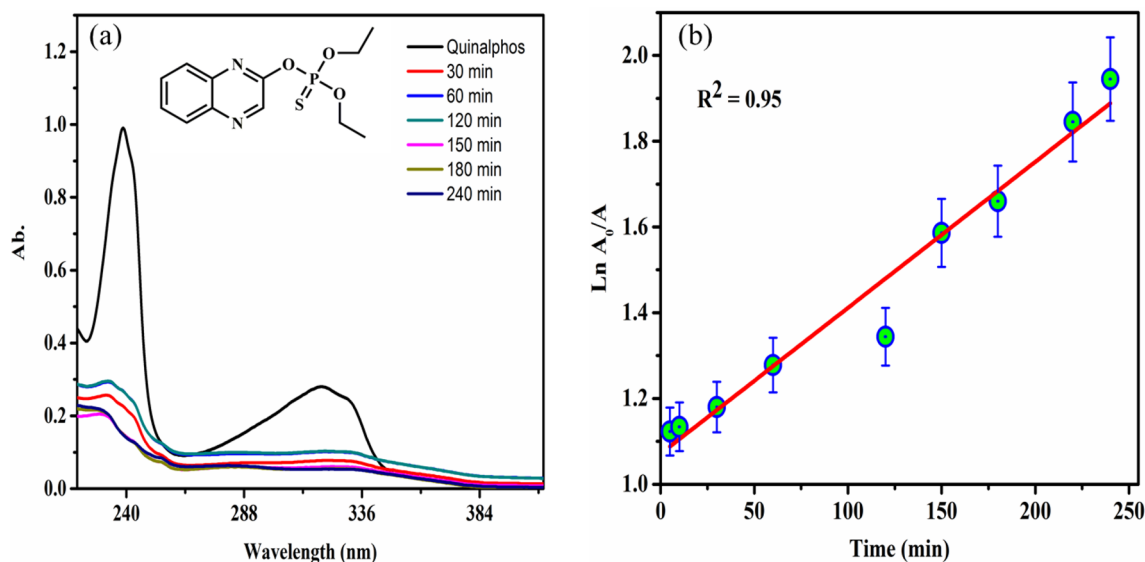


Fig. 11 Time dependent UV-Vis spectra (a) and Kinetic study and of photo-catalytic degradation of Quinalphos (b)

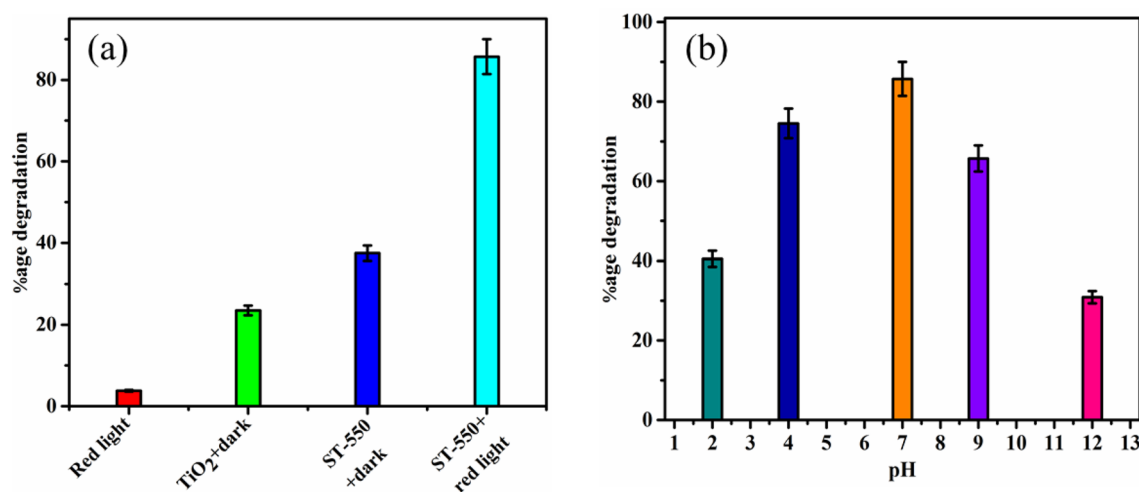


Fig. 12 Photocatalytic degradation of Quinalphos **a** under different conditions and **b** effect of pH under red light (660 nm)

that pH plays an important role in the degradation of pesticides. It has been spotted that as the pH increases the photocatalytic degradation with ST-550 increases and is displaying maximum degradation at 7 pH and afterward decreases. This can be explained based on the influence of alkaline pH on the surface state of catalysts and the generation of $\cdot\text{OH}$ free radicals.

Photocatalytic degradation of diclofenac

The photocatalyzed degradation reaction of Diclofenac was also investigated by changing various reaction conditions (pH and photolysis reaction). The change in absorption

maxima (275 nm) was used to examine the %age degradation of diclofenac.

The time-dependent photo-catalytic degradation of diclofenac with ST-550 under white light was confirmed by the UV-Vis spectrum (Fig. 13a). The characteristic absorption peak of diclofenac was observed at 275 nm. In the presence of S- TiO_2 , a gradual decrease in the intensity of absorption maxima was observed within 120 min and about 90.7% of the Diclofenac has been degraded.

According to the kinetic study, degradation of diclofenac followed the apparent first-order kinetic model (Fig. 13b). The correlation constant was found to be 0.9856 and the rate constant was 0.019 min^{-1} .

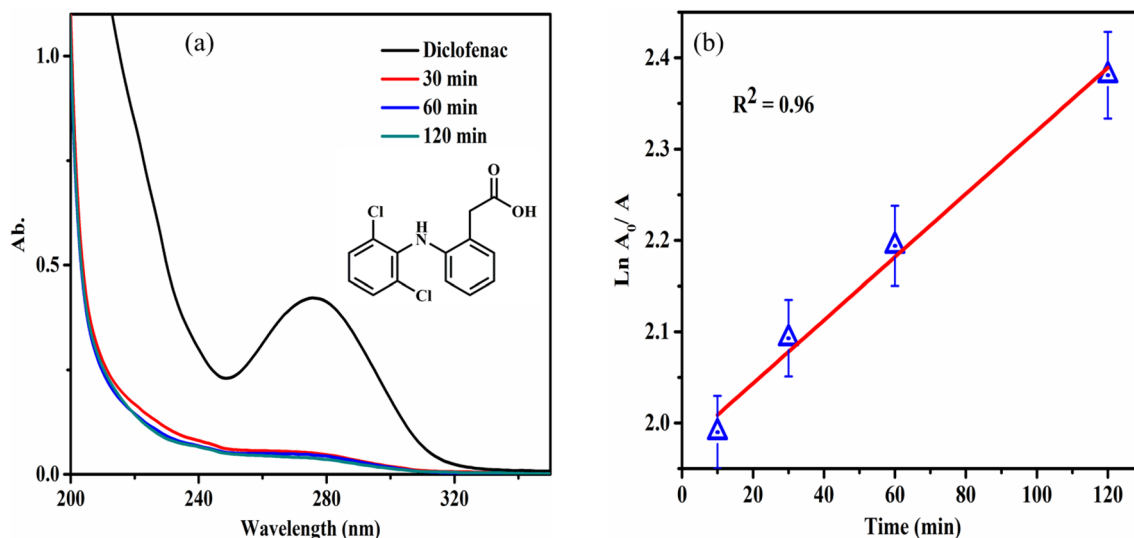


Fig. 13 Time-dependent UV–Vis spectra (a) and Kinetic study (b) of photocatalytic degradation of Diclofenac

The %age degradation of diclofenac was also studied at four different experimental conditions such as white light, undoped- TiO_2 / dark, ST-550/ dark, and ST- 550/ white light. The rate of degradation was studied at 275 nm (Fig. 14a), in the case of blank experimentation, only 7.8% of degradation was obtained under white light in absence of a catalyst. About 25.9% of diclofenac was degraded in dark with undoped- TiO_2 and 53.0% of diclofenac was degraded under dark conditions with ST-550. About 90.7% of the diclofenac degradation occurs by using ST-550 under white light.

The pH plays an important role to enhance the % degradation of organic pollutants (diclofenac) as shown in Fig. 14b. The results confirmed that as the pH of the diclofenac increases, the % degradation decreases and shows the maximum rate of degradation (90.7%) at pH 2 (Table 1).

Conclusion

The heterogeneous catalysis-based reaction provides an encouraging solution for the removal of various intolerant contaminants from the environment. TiO_2 is known as one of the most efficient photocatalysts due to its high stability toward photo corrosion, low cost, photo activity, and non-toxicity. TiO_2 absorbs a small amount of solar light because of its vast bandgap (3.2 eV). Hence, sulphur doping on TiO_2 lattice makes it visible light-responsive due to effective shift in a bandgap. Ultrasonic radiations-assisted synthesis of S-doped TiO_2 has been successfully carried out using thiophenol as a precursor of sulphur. Bandgap study data confirms the shift in response from the UV region to the visible region. The synthesized

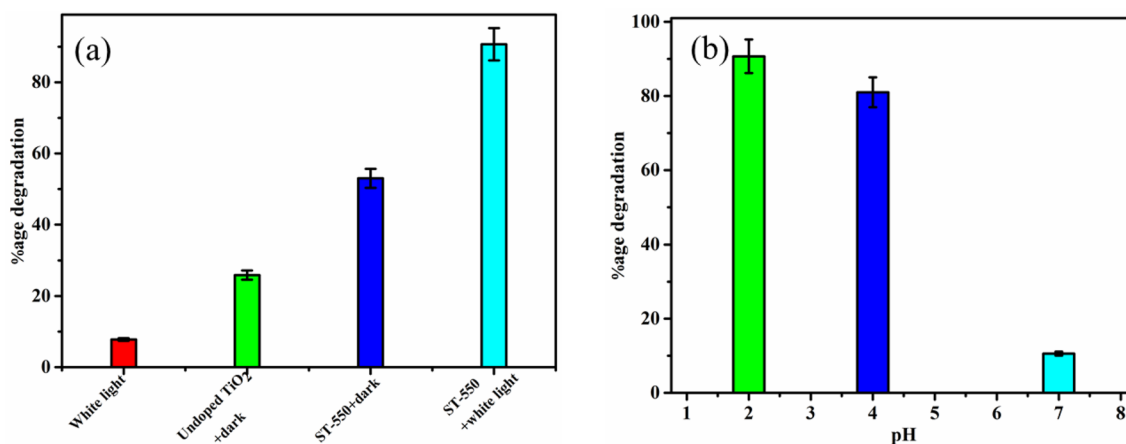


Fig. 14 Photocatalytic degradation of Diclofenac a under three different conditions and b effect of pH under white light (450 nm)

Table 1 Comparison of present work with the existing state of art

S. No	Catalyst	Target	Conditions	Degradation efficiency	References
1	S-TiO ₂ /rGO	Diclofenac	Solar irradiation	14.3%	[30]
2	N, S co-doped TiO ₂	Diclofenac	Visible light	90–95%	[31]
3	TiO ₂	Quinalphos	UV-A radiation	89.6%	[32]
4	Ce-TiO ₂	Quinalphos	Visible light	92%	[33]
5	Ag/TiO ₂ NTs	R6G	UV radiation	Not given	[34]
6	TiO ₂ @rGO	R6G	UV light	65%	[35]
7	S-TiO ₂	R6G	White light	91.7%	This work
		Quinalphos	Red light	85.7%	
		Diclofenac	White light	90.7%	

photocatalysts have a particle size in the nano range and are porous. The photocatalytic efficiency of S-doped TiO₂ was observed by degrading Rhodamine 6G, Quinalphos, and Diclofenac. The maximum degradation (91.7%) of the Rhodamine 6G, 85.7% of quinalphos, and 90.7% of the diclofenac were recorded with ST-550.

Acknowledgements The authors are thankful to the Director, Sant Longowal Institute of Engineering and Technology, Longowal, Punjab for providing essential assistance in conducting experimental work.

Declarations

Conflict of interest There is no conflict of interest to be declared.

References

- Almaguer MA, Cruz YR, da Fonseca FV (2021) Combination of advanced oxidation processes and microalgae aiming at recalcitrant wastewater treatment and algal biomass production: a review. *Environ Process* 8:483–509
- Garrido-Cardenas JA, Esteban-García B, Agüera A, Sánchez-Pérez JA, Manzano-Agugliaro F (2020) Wastewater treatment by advanced oxidation process and their worldwide research trends. *Int J Environ Res Public Health* 17(1):170
- Chen D, Cheng Y, Zhou N, Chen P, Wang Y, Li K, Huo S, Cheng P, Peng P, Zhang R (2020) Photocatalytic degradation of organic pollutants using TiO₂-based photocatalysts: a review. *J Clean Product* 268:121725
- Guo Y, Wen M, Li G, An T (2021) Recent advances in VOC elimination by catalytic oxidation technology onto various nanoparticles catalysts: a critical review. *Appl Catal B Environ* 281:119447
- Rekhate CV, Srivastava J (2020) Recent advances in ozone-based advanced oxidation processes for treatment of wastewater: a review. *Chem Eng J Adv* 3:100031
- Sharotri N, Sud D (2016) Ultrasound-assisted synthesis and characterization of visible light responsive nitrogen-doped TiO₂ nanomaterials for removal of 2-Chlorophenol. *Desalin Water Treat* 57(19):8776–8788
- Sharotri N, Sud D (2017) Visible light responsive Mn-S-codoped TiO₂ photocatalyst—synthesis, characterization and mechanistic aspect of photocatalytic degradation. *Sep Purif Technol* 183:382–391
- Piątkowska A, Janus M, Szymański K, Mozia S (2021) C-, N- and S-Doped TiO₂ photocatalysts: a review. *Catalysts* 11(1):144
- Ibrahim NS, Leaw WL, Mohamad D, Alias SH, Nur H (2020) A critical review of metal-doped TiO₂ and its structure–physical properties–photocatalytic activity relationship in hydrogen production. *Int J Hydrog Energy* 45:28553–28565
- Varma KS, Tayade RJ, Shah KJ, Joshi PA, Shukla AD, Gandhi VG (2020) Photocatalytic degradation of pharmaceutical and pesticide compounds (PPCs) using doped TiO₂ nanomaterials: a review. *Water-Energy Nexus* 3:46–61
- Al Zoubi W, Al-Hamdani AAS, Sunghun B, Ko YG (2021) A review on TiO₂-based composites for superior photocatalytic activity. *Rev Inorg Chem*
- Idrees F, Butt FK, Hammouda SB (2021) Progression in photocatalytic materials for efficient performance. *Multidisciplinary Digital Publishing Institute*
- Horikoshi S, Serpone N (2020) Can the photocatalyst TiO₂ be incorporated into a wastewater treatment method? Background and prospects. *Catal Today* 340:334–346
- El-Bery HM, Abdelhamid HN (2021) Photocatalytic Hydrogen Generation via Water Splitting using ZIF-67 derived Co₃O₄@C/TiO₂. *J Environ Chem Eng* 9:105702
- Abdellah AR, Abdelhamid HN, El-Adasy A-BA, Atalla AA, Aly KI (2020) One-pot synthesis of hierarchical porous covalent organic frameworks and two-dimensional nanomaterials for selective removal of anionic dyes. *J Environ Chem Eng* 8(5):104054
- Kassem AA, Abdelhamid HN, Fouad DM, Ibrahim SA (2020) Hydrogenation reduction of dyes using metal-organic framework-derived CuO@C. *Micropor Mesopor Mater* 305:110340
- Tongpool R, Setwong K (2008) Sulfur doping and its effect on TiO₂ photoactivity. *Songklanakarin J Sci Technol* 30(2):201–206
- Zhou M, Yu J (2008) Preparation and enhanced daylight-induced photocatalytic activity of C, N, S-tridoped titanium dioxide powders. *J Hazard Mater* 152(3):1229–1236
- Hamadani M, Reisi-Vanani A, Majedi A (2010) Synthesis, characterization and effect of calcination temperature on phase transformation and photocatalytic activity of Cu, S-codoped TiO₂ nanoparticles. *Appl Surf Sci* 256(6):1837–1844
- Ivanov S, Barylyak A, Besaha K, Bund A, Bobitski Y, Wojnarowska-Nowak R, Yaremchuk I, Kus-Liśkiewicz M (2016) Synthesis, characterization, and photocatalytic properties of sulfur- and carbon-codoped TiO₂ nanoparticles. *Nanoscale Res Lett* 11(1):1–12
- Ramacharyulu P, Nimbalkar DB, Kumar JP, Prasad G, Ke S-C (2015) N-doped, S-doped TiO₂ nanocatalysts: synthesis, characterization and photocatalytic activity in the presence of sunlight. *RSC Adv* 5(47):37096–37101

22. Sharotri N, Sud D (2015) A greener approach to synthesize visible light responsive nanoporous S-doped TiO₂ with enhanced photocatalytic activity. *New J Chem* 39(3):2217–2223
23. Hamadani M, Reisi-Vanani A, Majedi A (2009) Preparation and characterization of S-doped TiO₂ nanoparticles, effect of calcination temperature and evaluation of photocatalytic activity. *Mater Chem Phys* 116(2–3):376–382
24. Sun B, Smirniotis PG (2003) Interaction of anatase and rutile TiO₂ particles in aqueous photooxidation. *Catal Today* 88(1–2):49–59
25. Han C, Pelaez M, Likodimos V, Kontos AG, Falaras P, O’Shea K, Dionysiou DD (2011) Innovative visible light-activated sulfur doped TiO₂ films for water treatment. *Appl Catal B* 107(1–2):77–87
26. Ho W, Jimmy CY, Lee S (2006) Low-temperature hydrothermal synthesis of S-doped TiO₂ with visible light photocatalytic activity. *J Solid State Chem* 179(4):1171–1176
27. Szatmáry L, Bakardjieva S, Šubrt J, Bezdička P, Jirkovský J, Bastl Z, Brezová V, Korenko M (2011) Sulphur doped nanoparticles of TiO₂. *Catal Today* 161(1):23–28
28. Zhang W, Luo N, Huang S, Wu N-L, Wei M (2019) Sulfur-doped anatase TiO₂ as an anode for high-performance sodium-ion batteries. *ACS Appl Energy Mater* 2(5):3791–3797
29. Kumar KV, Porkodi K, Selvaganapathi A (2007) Constrains in solving Langmuir-Hinshelwood kinetic expression for the photocatalytic degradation of Auramine O aqueous solutions by ZnO catalyst. *Dyes Pigm* 75(1):246–249
30. Kovačić M, Perović K, Papac J, Tomić A, Matoh L, Žener B, Brodar T, Capan I, Surca AK, Kušić H (2020) One-pot synthesis of sulfur-doped TiO₂/reduced graphene oxide composite (S-TiO₂/rGO) with improved photocatalytic activity for the removal of diclofenac from water. *Materials* 13(7):1621
31. Irandost M, Akbarzadeh R, Pirsaeed M, Asadi A, Mohammadi P, Sillanpää M (2019) Fabrication of highly visible active N, S co-doped TiO₂@ MoS₂ heterojunction with synergistic effect for photocatalytic degradation of diclofenac: mechanisms, modeling and degradation pathway. *J Mole Liq* 291:111342
32. Sraw A, Toor AP, Wanchoo R (2016) Adsorption kinetics and degradation mechanism study of water persistent insecticide quinalphos: for heterogeneous photocatalysis onto TiO₂. *Desalination Water Treat* 57(36):16831–16842
33. Behera L, Barik B, Mohapatra S (2021) Improved photodegradation and antimicrobial activity of hydrothermally synthesized 0.2 Ce-TiO₂/RGO under visible light. *Colloid Surf A Physicochem Eng Aspect* 620:126553
34. Chong X, Zhao B, Li R, Ruan W, Yang X (2015) Photocatalytic degradation of rhodamine 6G on Ag modified TiO₂ nanotubes: surface-enhanced Raman scattering study on catalytic kinetics and substrate recyclability. *Colloids Surf, A* 481:7–12
35. Pu S, Zhu R, Ma H, Deng D, Pei X, Qi F, Chu W (2017) Facile in-situ design strategy to disperse TiO₂ nanoparticles on graphene for the enhanced photocatalytic degradation of rhodamine 6G. *Appl Catal B* 218:208–219

Publisher's Note Springer Nature remains neutral with regard to jurisdictional claims in published maps and institutional affiliations.